The influence of radiative feedback on star-formation

in the James Clerk Maxwell Telescope Gould Belt Survey of nearby star-forming regions.

Damian Jack Rumble

Submitted by Mr Damian Rumble to the University of Exeter as a thesis for the degree of Doctor of Philosophy in Physics, April, 2016.

I certify that all material in this thesis which is not my own work has been identified and that no material has previously been submitted and approved for the award of a degree by this or any other University.

Signed: .....

Mr D. J. Rumble

Date: .....

Abstract

I aim to show that I have spent three years usefully. Or maybe four.

Contents

List of Figures

List of Tables

Declaration

This thesis contains work published or pending publication as papers. Honest.

Acknowledgements

Hey.

Thanks.

ME
Exeter, U.K.
??th September 200?

1

Free-Free contamination

In this chapter we examine the arguments for a thermal Bremsstrahlung, or free-free, contribution to the SCUBA-2 detections, addressing questions regarding the source, strength, spectral index, and location of the turnover (from partially opaque to optically thin) of free-free emission. We examine the various sources of free-free emission in the JCMT GBS and asses the magnitude of the contribution of free-free to SCUBA-2 bands.

1.1 Introduction to thermal breemstralung emission

Thermal Bremsstrahlung, or free-free, emission is a thermal process by which photons are produced from electron scatter in a plasma in LTE. We derive the spectral index of the free-free emission by first considering the number of electrons, N_e, passing an ion, per unit time. The electrons have a speed range v to $v + dv$ and the the ion has an impact parameter of b to $b + db$ such that

$$N_e(2\pi b\, db)v f(v)\, dv. \tag{1.1}$$

In this system the number of 'encounters', $N(v, b)$, between the ion and an electron, per unit volume, per unit time, is

$$N(v, b)\, dv\, db = (2\pi\, db)[v f(v)]N_e N_i, \tag{1.2}$$

and the average energy per unit frequency, W_ν, is

$$W_\nu \approx \frac{\pi^2}{2}\frac{Z^2 e^6}{c^3 m_e^2}\left(\frac{1}{b^2 v^2}\right) \tag{1.3}$$

where the above constants have their usual meanings. From radiative transfer, the emission coefficient, ϵ_ν, can be calculated by integrating energy and encounters over b and v as such,

$$4\pi\epsilon_\nu = \int_{b=0}^{\infty}\int_{v=0}^{\infty} W_\nu(v,b)N(v,b)\,dv\,db. \tag{1.4}$$

Considering non-relativistic Maxwellian distribution of electron velocities,

$$f(v) = \frac{4v^2}{\sqrt{\pi}}\left(\frac{m_e}{2k_BT_e}\right)^{3/2} exp\left(-\frac{m_ev^2}{2k_BT_e}\right), \tag{1.5}$$

the free-free emission coefficient can be derived as

$$\epsilon_\nu = \frac{\pi^2Z^2e^6N_eN_i}{4c^3m_e^2}\left(\frac{2m_e}{\pi\,k_BT_e}\right)^{1/2} ln\left(\frac{b_{max}}{b_{min}}\right). \tag{1.6}$$

The minimum and maximum impact parameters, $b_{min}(v)$ and $b_{max}(v,\nu)$, make up the Gaunt factor,

$$g_{ff}(\nu,T) = \frac{\sqrt{3}}{\pi} ln\left(\frac{b_{max}}{b_{min}}\right), \tag{1.7}$$

that value of which ranges as $g_{ff}(\nu) \propto 1/\nu$ between 1 and 10 across the radio spectrum. Using Kirchoff's law ($\kappa_\nu = \epsilon_\nu/B_\nu(T)$) the absorption coefficient, κ_ν, can be calculated in the Rayleigh-Jeans limit as

$$\kappa_\nu = \frac{1}{\nu^2T^{3/2}}\frac{\pi^3}{\sqrt{48}}\,g_{ff}\left[\frac{Z^2e^6}{c}N_eN_i\frac{1}{\sqrt{2\pi\,(m_ek_B)^3}}\right]. \tag{1.8}$$

Because the Gaunt factor is weakly inversely proportional to frequency the opacity of free-free emission can be approximated to $\kappa_\nu \propto \nu^{-2.1}$ (Oster, 1961; Altenhoff et al., 1970) and as a result the optical depth of the free-free can be written as

$$\tau_\nu \approx \int \frac{N_e^2}{\nu^{2.1}T^{3/2}}\,ds. \tag{1.9}$$

From this expression it can be determined that at low frequencies $\tau_\nu \gg 1$ and emission will become optically thick. Likewise at very high frequencies emission will become optically, $\tau_\nu \ll 1$. Considering the equation of flux density from radiative transfer,

$$S_\nu = \int_\Omega B_\nu(T,\nu)\tau\,d\Omega, \tag{1.10}$$

it is possible to show that free-free emission at very low frequencies will resemble a black body where $S_\nu \propto \nu^2$. Likewise at very high frequencies free-free emission is approximately flat, $S_\nu \propto \nu^{-0.1}$ (Mezger & Henderson, 1967).

At $\tau_\nu = 1$ free-free emission will undergo a 'turnover' from the optically thick to thin regime, typically at low frequencies around KHz regime. At very high frequencies another break occurs in the spectrum when $h\nu \gg k_BT_e$ and the free-free spectrum goes from flat to an exponential

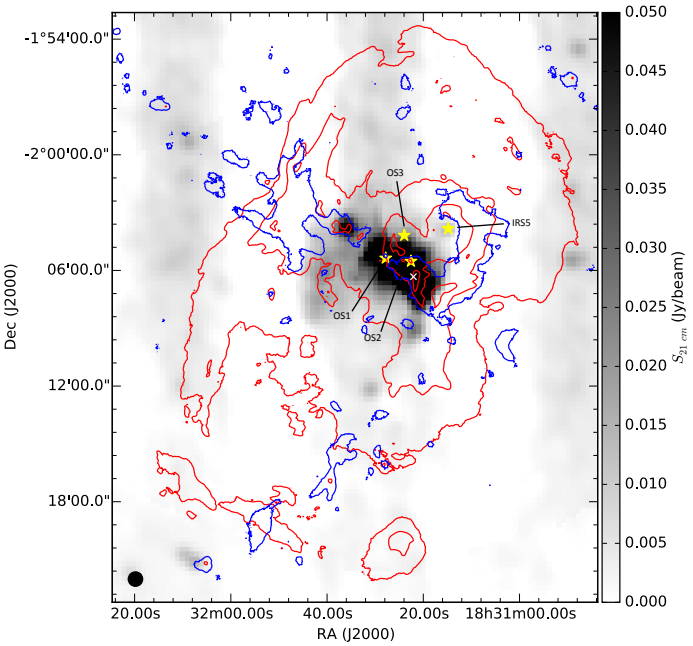

Figure 1.1: Archival VLA 21 cm NRAO VLA Sky Survey (Condon & Kaplan, 1998) continuum map of the W40 complex H II region (45″ resolution). Red *Herschel* 70 μm contours of the nebulosity SH-64 at 300, 1200, 4800, 12000 MJy/Sr. Blue SCUBA-2 850 μm contours of the dust cloud at the 5σ level. Yellow stars indicate the locations of the OB stars, with the O9.5 star OS1 the primary ionising object of the region. The white cross indicates the peak of the VLA 21 cm emission.

decay that is described by,

$$J_{\nu,T} \propto T^{-1/2} exp\left(\frac{-h\nu}{k_B T_e}\right) N_e^2 g_{ff}(\nu, T), \tag{1.11}$$

where $J_{\nu,T}$ is the emissivity [CITE]. For a electron temperature of 10^4 K, the exponential decay break can be estimated at occurring short ward of 1 μm.

1.2 H II observations

In star formation, free-free emission is typically observed from H II regions formed by photoionisation of molecular hydrogen by UV photons from B4V stars or earlier. The UV, or Lyman, photon density, N_{Ly}, required to maintain the ionisation of an H II region is given by Kurtz et al. (1994) as

$$N_{Ly} \geq 8.04 \times 10^{46} T_e^{-0.85} U^3, \tag{1.12}$$

where U is the excitation parameter $R_s N_e^{2/3}$ for a Stromgern sphere of radius R_s. These two variables are also related through

$$N_{Ly} = \alpha_H N_e^2 \frac{4}{3} \pi R_s^3 \tag{1.13}$$

where α_H is the hydrogen recombination rate, approximately equal to $3{\times}10^{-13}\,\mathrm{cm^3\,s^{-1}}$. H II regions are large scale, low density structures with radii greater than 10^{18} cm and N_e less than $10^4\,\mathrm{cm^{-3}}$. The stellar N^*_{Ly} for the OB stars capable of producing H II regions is typically greater than $10^{46}\,\mathrm{cm^{-3}}$. By considering N^*_{Ly} at specific frequencies Kurtz et al. (1994) calculates the flux density that would be observed if viewing an H II region at a distance, d, using

$$S_\nu(\mathrm{Jy}) = 1.32\times10^{-49}\xi N^*_{Ly} a(\nu,T)\left(\frac{\nu}{\mathrm{GHz}}\right)^{-0.1}\left(\frac{T_e}{\mathrm{K}}\right)^{0.5}\left(\frac{d}{\mathrm{kpc}}\right)^{-2}, \tag{1.14}$$

where a(ν, T) is a constant equal to 0.98 (Mezger & Henderson, 1967) and ξ is the fraction of UV photons not absorbed by the dust set at 10%. Free-free emission from large scale, diffuse H II regions is predicated to be optically thin at radio frequencies emission where the power law becomes approximately flat with an α_{ff} = -0.1 (Oster, 1961; Mezger & Henderson, 1967).

In an H II region UV heat up the gasses and plasma of the ISM by radiative transfer to temperatures in excess of 10000 K. This causes the exposed material to expand adiabatically into the space surround the OB star/s. In the transition zone between the H II region and the neutral ISM two fronts are observed; the ionisation front [CITE] and the shock [CITE]. In the shock front, expansion of the H II region is thought to sweep up the ISM producing localised over densities associated with a 'shell' of material around the H II region [CITE]. Whether the shock front has sufficient pressure to destabilise existing cores within any exposed filaments and 'trigger' star-formation is an open question (Lefloch & Lazareff, 1994; Urquhart et al., 2009). The ionisation front represents a region where neutral material is being ionised through exposure to UV photons. Rate of ionisation is heavily dependant on the local density. High density regions take considerably longer to break down than lower density regions and as a result 'champagne' flows (Dale et al., 2012) are observed where the molecular cloud has been ruptured by an internal H II and photons are exiting through a narrow opening. The H II region can be further imbedded by accretion flow of neutral material onto the star Dale et al. (2005); Dale & Bonnell (2011) and by gravity when at the centre of massive cloud Yorke et al. (1989). The region in-between the ionisation front and shock front is collectively known as a photo-dissociative region (PDR, Thompson et al. 2004). An example of a PDR is observed in Perseus, a star forming region observed as part of the JCMT GBS.

1.3 UCH II observations

In addition to these large scale structures, free-free emission is also detected in the form of a power law at scale sizes comparable to individual stars (Panagia & Felli, 1975).

Early type OB stars undergoing mass loss through winds produce free-free emission from ionised material leaving the star, in addition to UV photons ionising the ISM, and are considered compact (≤0.5 pc), ultra compact (≤ 0.1 pc) and hyper compact (≤ 0.03 pc) H II regions (Wright & Barlow, 1975; Harvey et al., 1979). These are the processors of evolved H II regions (10 pc,Kurtz 2005). From here on in we refer to these classes collectively as UCH II regions. Whereas H II regions are diffuse, homogenous fields of emission, UCH II regions have an electron density is

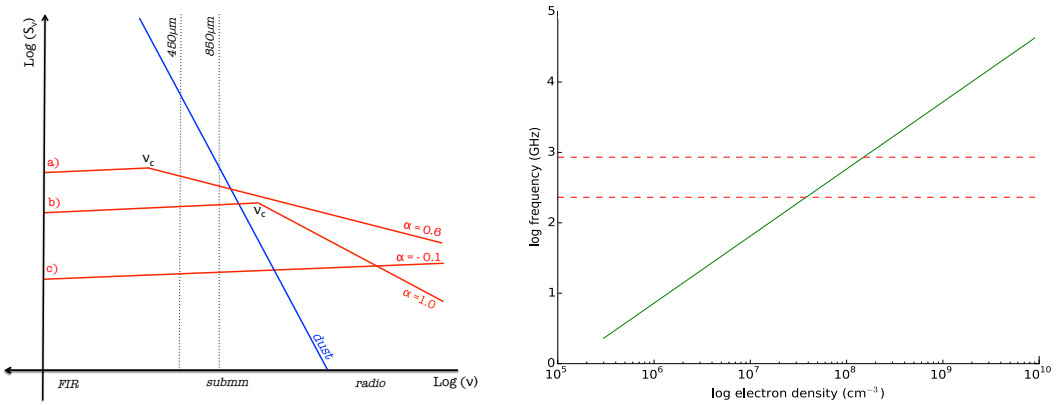

Figure 1.2: **Left]** A schematic of the SED shape for three hypothetical scenarios offig:freefreealpha free-free emission. **Case a)** an UCH II with $\alpha_{\rm ff}$ = 0.6 has a turnover that occurs short ward of the submillimetre regime, and as a result has a majority contribution to the 850 μm band and a significant contribution to the 450 μm band. **Case b)** a YSO emits free-free emission, $\alpha_{\rm ff}$ = 1.0, from a collimated jet. However the spectrum turns over to the optically thin regime long ward of submillimetre wavelengths, and consequently free-free emission contributes roughly equally to both SCUBA-2 bands. **Case c)** a H II region has free-free emission from diffuse gas of $\alpha_{\rm ff}$ = -0.1 that outshines that from compact objects at long wavelengths. However, the flat spectrum means that at submillimetre wavelengths the emission is all but negligible. **Right]** Free-free turnover as a function of launching electron density (as described by Olnon 1975 in Equation 1.15). Dashed lines indicate the submillimetre regime (1.3 mm to 350 μm).

inversely proportional to radius. Assuming spherical winds of constant velocity Panagia & Felli (1975) and Wright & Barlow (1975) derive the spectral index of the free-free emission as $\alpha_{\rm ff}$ = 0.6. Large surveys of UCH II candidate regions are consistent with this result (Harvey et al., 1979; Wood & Churchwell, 1989; Kurtz et al., 1994; Molinari et al., 1998; Walsh et al., 1998; Kurtz, 2005).

Where the free-free emission mechanism is a spherical ionised stellar wind,Emission can be thought of as *partially thick* with lower frequencies probing greater depths of emission within the wind before becoming fully optically thin at shorter wavelengths where only the diffuse H II region is being observed. The exact location of this free-free turnover, ν_c, has been much debated in the literature. If the turnover occurs short-ward of submillimetre wavelengths then it is possible that the free-free may contribute in part to SCUBA-2 observations of dust emission. Olnon (1975) defines ν_c as a function of electron density, $N_e(R) = N_{e,0}$ where r ≤ R, as

$$\log_{10} \nu_c = -0.516 + \frac{1}{2.1} \log_{10} \left(\frac{8}{3} R N_{e,0}^2 T_e^{-1.35} \right), \tag{1.15}$$

where R is the launching radius of the wind (typically 10 AU) and T_e is the electron temperature (typically 10^4 K). Figure **??** highlights how a turnover point short wards of the submillimetre regime requires an electron density in excess of 10^8 cm^{-3}.

The electron density n_0 is not easily determined from observations. We therefore turn to indirect measurements to make a general statement about what systems will produce free-free emission that is opaque at submillimetre wavelengths and hence may subsequently be contributing

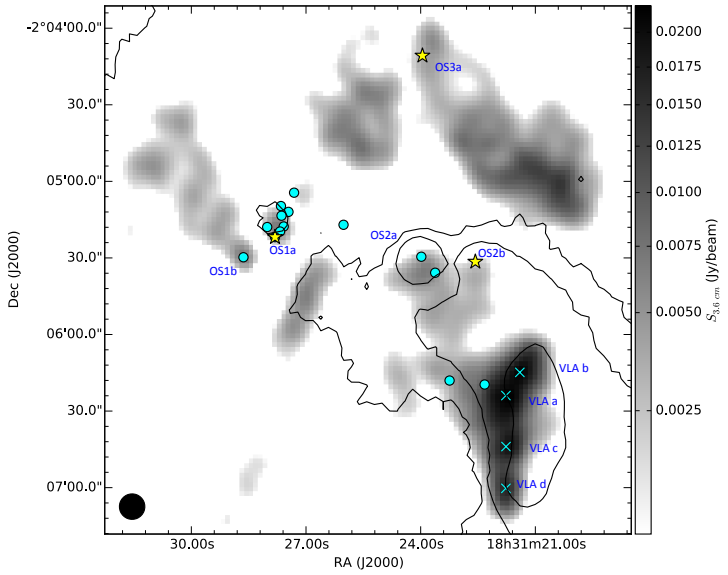

Figure 1.3: Archival AUI/NRAO 3.6 cm map of the W40 complex OB association (NRAO/VLA Archive Survey, (c) 2005-2007). SCUBA-2 850 μm contours of dust emission at 5σ, 15σ and 50σ overlaid. Yellow markers indicate the locations of the OB stars while cyan circles indicate the location of compact radio sources identified by Rodriguez et al 2010. Cyan crosses mark the four peaks identified separately in the AUI/NRAO 3.6 cm map.

to SCUBA-2 emission. We assume that n_0 is proportional to stellar mass and by association varies with spectral class as the more massive stars are known to produce more vigorous winds and greater mass loss. Sandell et al. (2011)'s results indicate that the free-free contribution is significant for early B stars in their sample, but not for late B and A class stars. MWC 297 is the lowest mass star in their sample for which free-free contributes at SCUBA-2 wavelengths and we therefore mark it as a lower limit of stellar class. MWC 297 has a luminosity of 3×10^3 $L_\odot$ (Drew et al., 1997) which corresponds to a class B1.5Ve or B4V star. Given the nature of these assumptions, we are limited to assigning an upper estimate of spectral class B4V, above which the free-free turnover can occur in the submilimetre regime.

UCH II are associated with stars that are sufficiently massive (greater than $8M_\odot$) that their Kelvin-Helmholtz contraction timescale is shorter than their free fall and accretion timescale (Manoj et al., 2007). These stars reach the main sequence and start producing ionising radiation whilst still embedded within their protostellar envelope (McKee & Tan, 2003). This would then lead to a compact region of highly ionised winds, as detected by Malbet et al. (2007) and Drew et al. (1997). We follow Wood & Churchwell (1989)'s description of an UCH II region as region with electron density greater than 10^4 cm^{-3} within a diameter of less than 0.1 pc. The minute size of the UCH II region means they cannot be detected optically and are interest observed through free-free processes or the indirect heating of dust. The lifetime of the ultra-compact stage of an H II region is estimated at $4{\times}10^5$ years, approximately 10% the lifetime of a typical O star.

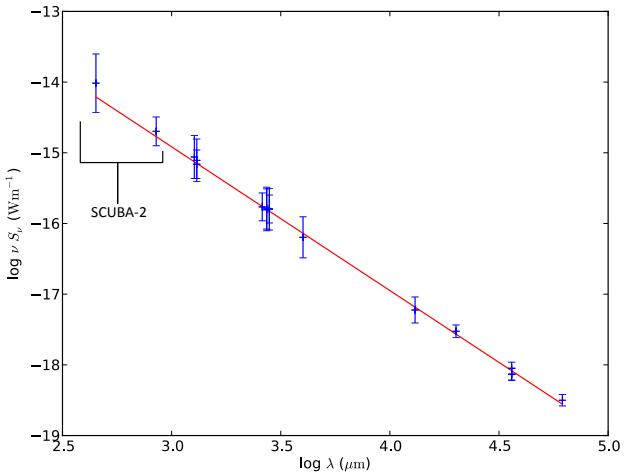

Figure 1.4: The Spectral Energy Distribution of MWC 297 from submillimetre to radio wavelengths. SCUBA-2 fluxes (found using aperture photometry as described in Section 5.2.) are presented alongside those collated by Sandell et al. (2011) who fit a power law $\alpha = 1.03 \pm 0.02$, consistent with free-free emission from an UCHII region and polar jets or outflows.

1.3.1 Jets

A minority of radio bright young OB stars are observed with $\alpha_{\rm ff} \geq 0.6$, for example MWC 349 (Olnon, 1975), MWC 297 Skinner et al. (1993); Sandell et al. (2011) and AB Aur (Rodríguez et al., 2014). Reynolds (1986) provides a comprehensive examination of models for stellar winds and finds that, where the outflow is highly collimated and accelerating (as this the case of bi-polar jets) the spectral index becomes increasingly opaque with $\alpha_{\rm ff} \simeq 1.0$. [CAN DERIVE IF NECESSARY BUT ITS PRETTY OVERKILL].

MWC 349 (Tafoya et al., 2004; Sandell et al., 2011) and MWC 297 (Sandell et al., 2011; Rumble et al., 2015) are early B-class Herbig stars where empirical observations have suggested that the free-free emission is sufficiently bright and opaque that it dominates over the dust emission at submillimetre wavelengths and produces a distinct point source in the observations consistent with a compact object. If similar point sources are present the SCUBA-2 observations of W40 complex, and are also consistent the location of whole compact radio sources, that could well signify the potential for free-free contribution.

1.4 Free-free contribution to SCUBA-2

Where free-free emission is significantly bright and remains optically opaque up to submillimetre wavelengths it may be detected by SCUBA-2 in the 450 and 850 μm bands.

Harvey et al. (1979), Kurtz et al. (1994) and Sandell et al. (2011) present multi-wavelength radio surveys of numerous HAeBe systems. A number of A class and late B class stars have faint free-free UCH II detections that appear to become optically thin long-ward of the submilimetre regime or are otherwise negligible when compared to emission at from the dust in the protostellar disc or envelope. Rodríguez et al. (2014) finds evidence that free-free emission in AB Aur has

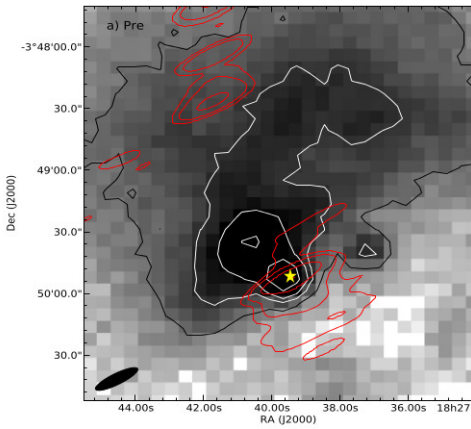

in MWC297/mwc297$_a$rXiv/MNRAS/20140618$_m$wc297$_c$ontamination.jpeg

Figure 1.5: IR1 SCUBA-2 850 μm data before *left* and after *right* removal of free-free contamination from an UCHII region and polar jets/winds (represented by the point source contours in the *left* plot). SCUBA-2 contours are at 0.011, 0.022, 0.033 and 0.055 Jy/pixel (corresponding to 5, 10, 15 and 25 σ detection limits). 6 cm VLA contours (red) from Sandell (private comm.) at 0.002, 0.005, 0.02, 0.072, 0.083 Jy/beam are overlaid on the left hand panel. The location of MWC 297 is marked with a star. Beam sizes are shown at the bottom of the image (VLA CnD config. *left* and JCMT *right*.)

index $\alpha_{\rm ff} = 1.1$ at cm wavelengths, however flux becomes optically thin by 1.3 mm, leading to the conclusion that $\nu_c \sim 70$ GHz. The early B systems of MWC 349, MWC 279 and LkHα 101 are observed to have strong free-free wind or jet emission which fits a power law right up to the submillimetre where the free-free provides a substantial, if not the majority of emission at these wavelengths. Olnon (1975) calculates that $\nu_c \sim 575$ GHz for MWC 349 using Equation 1.15, given that R $\sim$ 11 AU and $N_{e,0} \sim 9{\times}10^8$ cm^{-3} (Greenstein, 1973). Harvey et al. (1979) goes further and argues that free-free emission may be opaque up to 100 μm.

We present our methods for calculating and subtracting the free-free contribution from SCUBA-2 data published in Rumble et al. (2015) and Rumble et al. (2016, in prep.).

1.4.1 Direct methods

Skinner et al. (1993) studied free-free 3.6 cm and 6.0 cm radio emission from stellar winds around the B1.5ve star MWC 297 and found a power law of the form $S_\nu \propto \nu^\alpha$ where α is equal to 0.6238 in the optically thin regime. Sandell et al. (2011) extended the study down to 3 mm and revised the spectral index to $\alpha = 1.03 \pm 0.02$ which is consistent with a collimated jet component to free-free emission. The free-free power law extends into the submillimetre spectrum; however, at wavelengths shorter than 2.7 mm there is potential for a thermal dust component in the observed flux, so submillimetre flux is not included in the calculation of α.

Figure 1.5 displays 6 cm radio emission from the VLA CnD configuration in conjunction with SCUBA-2 850 μm data (Skinner 1993, Sandell priv. comm). Both sets of data show peaks in emission which are coincident with a point source at the location of the star MWC 297 in 1 mm and 3 mm data presented by Alonso-Albi et al. (2009). The peak of the SCUBA-2 850 μm

emission in Figure 1.5 is 86 mJy/pixel, consistent with the SCUBA 850 μm value of 82 mJy/pixel (Alonso-Albi et al., 2009).

The VLA data also show extended emission to the north and south of MWC 297 which is consistent with polar winds or jets. The intensity of emission is significantly weaker than that of the UCHII region. Considering the elongated beam shape of the VLA CnD observations (21.1″× 5.2″, PA= −61°.3) accounts for much the E/W elongation of the emission. In addition to this, Manoj et al. (2007) describe this emission as coming from within 80 AU of MWC 297. This is much smaller than the JCMT beam and therefore we model the dominant free-free emission from MWC 297 as a point source.

By taking the revised power law least square fit to Skinner et al. (1993) and Sandell et al. (2011)'s results at radio and millimetre wavelengths and extrapolating to the submillimetre wavelengths of SCUBA-2, we are able to calculate the effect of free-free emission due to a point-like UCHII region as an integrated flux of 934±128 mJy at 450 μm and 471±62 mJy at 850 μm. Single pixels with these values were then implanted into blank SCUBA-2 450 and 850 μm PONGs and the map convolved with the JCMT beam to produce an SCUBA-2 free-free emission map. These are subtracted off of the original SCUBA-2 maps to leave a SCUBA-2 dust map.

In addition to small scale free-free structures that are modelled as point sources, we can also run a free-free subtraction for large-scale emission from the diffuse emission from the H II region.

Archival VLA 21 cm data (45″ resolution) is presented in Figure 1.1 and shows the location of the 1.7′ large scale H II region associated with SH-64 (Condon & Kaplan, 1998). Rodney & Reipurth (2008) presents a summary of observations at multiple radio wavelengths and conclude a flat spectral index (α = -0.1) as expected from homogenous, optically thin free-free emission as predicted by Oster (1961) and Mezger & Henderson (1967).

Using a simple gaussian we convolve the SCUBA-2 850 μm up to the 45″ resolution of the VLA data so the fluxes are comparable. Likewise we re-grid the data on to a common pixel size. SCUBA-2 data has large scale structure greater than 5′ removed during the data reduction process so we use the FINDBACK tool (see Section 2) to mimic the process on the VLA data. The VLA fluxes are subsequently scaled up to 850 μm following an α = -0.1 before they are subtracted from the SCUBA-2 observations.

1.4.2 Indirect methods

In the previous section we were able to combine observations across a range of wavelengths to directly and accurately calculate the free-free spectral index. Other regions have been less well studied in high resolution and radio catalogues exist only for single wavelengths from which it is not possible to directly calculate $\alpha_{\rm ff}$. In order to get around this problem we can asses the radio properties of any free-free sources to determine whether or not it can be classified as H II, spherical wind UCH IIor collimated jet UCH II region. By considering the spectral class (if known) of the source and SCUBA-2 observations we can also make a judgement on whether or not any free-free emission is optically thick or thin at submillimetre wavelengths. In this way we can indirectly estimate the extent the free-free contribution to SCUBA-2 observations in more regions.

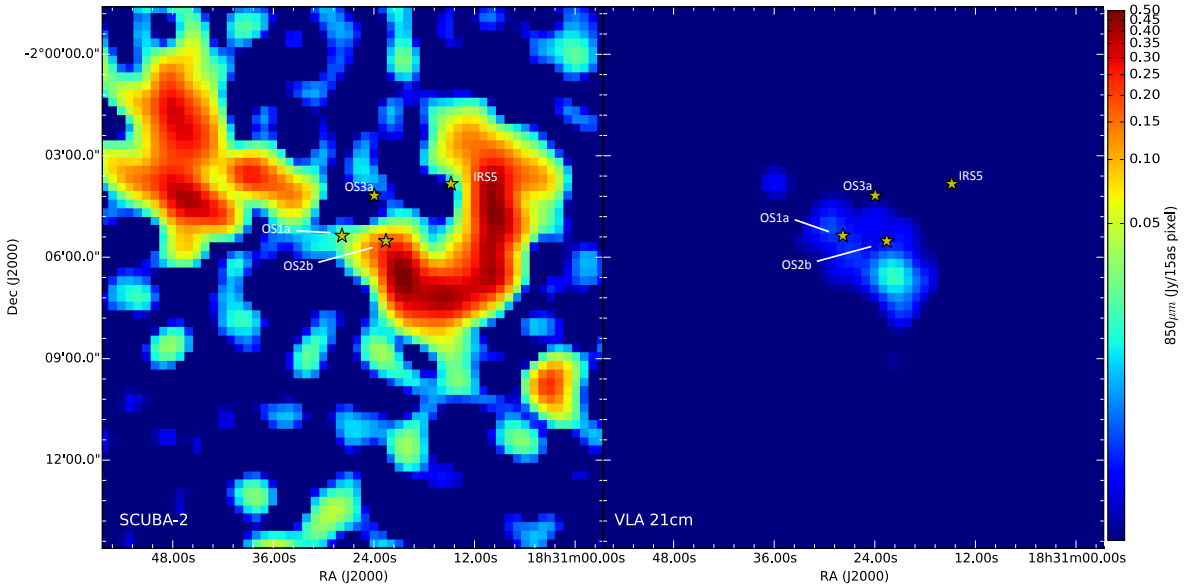

Figure 1.6: The free-free contribution from large-scale H II gas, modelled using archival VLA 21 cm observations (Condon & Kaplan, 1998) assuming $\alpha_{\rm ff}$ = -0.1 (right), compared to SCUBA-2 dust emission at 850 μm (left). Maps have common 15″ pixels and 45″ resolution. Markers indicate the locations of the OB stars.

Table 1.1: Summary of radio findings on bright objects in W40.

Source	2MASS ID	Type	Time variable 3.6 cm?	Associated jet?	SCUBA-2 point source?	Free-fre optically th
OS 1a (North)	18312782-0205228	Herbig AeBe	N	N	Y	?
OS 1a (South)	18312782-0205228	O9.5	-	N	Y	-
OS 1b	18312866-0205297	Class II	N	Y	N	N
OS 1c	18312601-0205169	Class II	Y	N	N	N
OS 2a	18312397-0205295	Herbig AeBe	Y	?	Y	?
OS 2b	18312257-0205315	B4	Y	N	Y	?
OS 3a	18312395-0204107	B3*(binary)	-	-	N	-
IRS 5	18311482-0203497	B1	-	-	N	N

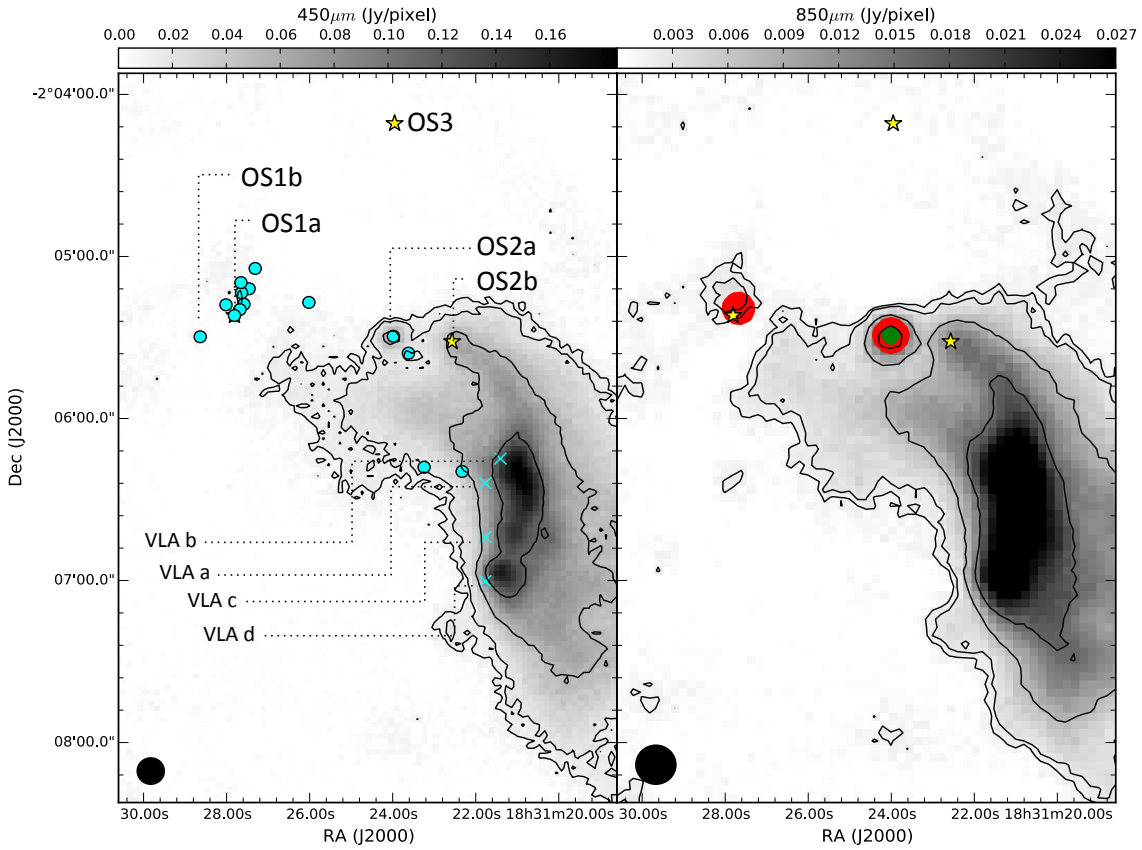

Figure 1.7: The free-free contribution of compact radio sources OS1a and OS2a at 450 μm (left) and 850 μm (right), modelled as point sources extrapolated from the Rodriguez et al. 2010 3.6 cm fluxes with assumed spectral indices given in Table 1.3. Yellow markers with thick outlines indicate the locations of the OB stars, cyan circles the location of all the Rodriguez et al. 2010 compact radio sources and cyan crosses the location of four peaks identified separately in the AUI/NRAO 3.6 cm map (450 μm only). Black contours trace SCUBA-2 data at 3σ, 5σ, 15σ and 30σ. Red and green filled contours trace the free-free contribution at 3σ and 5σ from optically thick (see Table 1.1).

In the W40 complex archival AUI/NRAO 3.6 cm data is used and presented in Figure 1.3. The coverage of this region is limited approximately 5′ and resolution of 9.97″ is comparable to SCUBA-2. As a result AUI/NRAO 3.6 cm is not able to resolve individual sources but can pick up extended radio emission associated with outflows. Rodríguez et al. (2010) supplement these data with high-resolution photometry at the same wavelength but with a reduced coverage of 4′.

No additional observations of alternative wavelengths at comparable resolution are available to this author, therefore it is not possible to empirically measure the free-free spectral index and we turn to indirect methods to infer $\alpha_{\rm ff}$. This requires examining the evidence for sufficient electron density, N_e, for any free-free emission to remain optically thick up to the submillimetre regime, and for features that hint that the host star may power a jet.

The W40 complex contains a number of massive star and Shuping et al. (2012) conduct a NIR study of the brightest objects in W40, identifying a list of one late O star, 3 B stars, 2 Herbig AeBe stars and 2 low mass Class III YSOs. These objects are listed in Table 1.1 and build on early IR studies by Smith et al. (1985). Rodríguez et al. (2010) resolves 20 compact radio sources, 15 of which are consistent with 2MASS sources and, by using time-variability, is able to classify 8, variable, YSOcs and 7, non-variable, UCH II candidate regions. Rodríguez et al. (2010) also identify non-compact radio sources without IR counterparts and these are interpreted as shock fronts from thermal jets that were likely formed by the local HAeBe stars OS1b and OS2a/b.

The example early B systems of MWC 349, MWC 279 and LkHα 101 (Sandell et al., 2011) all have free-free emission that is opaque at submillimtere wavelengths which can be identified as a bright peak in SCUBA observations. The lack of a bright submillimetre point source consistent with the candidate UCH II would likely signify that free-free emission turns over too early, or that emission is not bright enough to have a significant impact on the total flux density observed by SCUBA-2. This test immediately rules out OS1b, c, OS3a and IRS 5 from having significant UCH II regions as they are not detected in SCUBA-2 at either wavelength.

OS1 and OS2a, presented in Figures 1.1 and 1.3 have coincident SCUBA-2 emission so in these cases we make the initial assumption that 100% of emission at SCUBA-2 850 μm is produced by free-free and measure the subsequent spectral index. This initial assumption is subsequently adjusted until a spectral index that fitted a model of $\alpha_{\rm ff} \sim$ -0.1, 0.6 or 1.0. Photometry from SCUBA-2 450 and 850 μm and AUI/NRAO 3.6 cm maps was conducted with a 14.5″ aperture (the SCUBA-2 850 μm beam FWHM). Rodríguez et al. (2010) also detects time variability of radio emission from a number of radio sources in the W40 complex, concluding that a variable detection is symptomatic of episodic accretion processes and non-variable emission are a result of an UCH II region. They also detect a number of irregular radio without an IR detection which they interpret at shocks from jet outflows. We use these as further tools to indirectly infer whether or not a YSO has an UCH II region and/or jet.

OS1 is a close cluster of objects that are not resolved by SCUBA-2 or the AUI/NRAO beam but are listed as a number of objects in Rodríguez et al. (2010), four of which have none-variable emission indicating an UCH II region. There is also no significant emission at 450 μm which suggests that if there is any free-free contribution at 850 μm, the emission has become optically thin by 450 μm. An $\alpha_{\rm ff}$ = 0.6 represents emission of 6.36 mJy of free-free at 850 μm, a

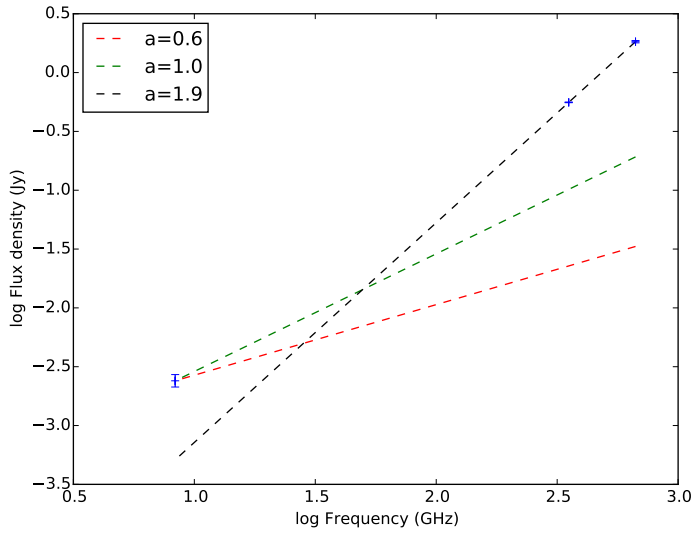

Figure 1.8: Modelling free-free emission in OS2a from the Rodriguez et al. (2010) 3.6 cm data for a given $\alpha_{\rm ff}$ = 0.6 (red), 1.0 (green), and the observed dust spectral index (black).

50% contribution. This result is consistent with the presence of HAeBe stars in the cluster. No jet shocks are found in the vicinity of the cluster and so we rule out the collimated jet configuration of free-free emission.

OS2a is a single HAeBe star that is resolved as a strong point source by SCUBA-2 at both 450 μm and 850 μm. Rodríguez et al. (2010) does resolve both OS2a at 3.6 cm and therefore these fluxes are used to complete the contribution test. Two results are returned; an $\alpha_{\rm ff}$ = 0.6 represents a 5% contribution (1.86 mJy) and an $\alpha_{\rm ff}$ = 1.0 represents a 22% contribution (8.18 mJy). OS2a is variable in nature but it also has nearby shock fronts which are consistent with active accretion, so the jet scenario of $\alpha_{\rm ff}$ = 1.0 appears the more likely outcome. No spectral class is available for this object. Both tests infer that even if the free-free emission is opaque at SCUBA-2 wavelengths, the SCUBA-2 source is remains dominated by dust emission. These results, and others, are summarised in Table 1.1. OS2b has a SCUBA-2 peak at both wavelengths but given its spectral class of B4 we consider it unlikely that any free-free emission will remain optically thick in the submillimetre regime.

In addition to this radio catalogue, we identify four radio peaks in Archival AUI/NRAO 3.6 cm map which were outside of the coverage of Rodríguez et al. (2010) which are marked in Figure 1.3 as VLAa, b, c and d. As there is no clear point source in the SCUBA-2 maps we assume that these additional VLA radio sources are optically thin at these wavelengths and take no further action.

Table 1.2: Summary of free-free contributions to SCUBA-2 wavelengths from MWC 297. The uncertainty on flux density at 450 μm is 0.03 Jy and 850 μm is 0.0025 Jy.

	3.6 cm (Jy)	450 μm (Jy)				850 μm (Jy)				
Object	VLA[a]	SCUBA-2	Free-free	Dust	%	SCUBA-2	Free-free	Dust	%	α_{f}
MWC 297	0.0099	0.1886	0.1377	0.0510	73±5	0.0860	0.0709	0.0150	82±4	1.0

1.5 The free-free contribution in Serpens MWC 297 results and discussion.

We determine that free-free emission from an UCHII region and polar jets/winds associated with MWC 297 contaminates the 450 μm and 850 μm data (Skinner et al., 1993). The nature of the free-free emission from the outflow has been debated by various authors. Malbet et al. (2007) and Manoj et al. (2007) argue for ionised stellar winds that dominate at higher latitudes, whereas Skinner et al. (1993) and Sandell et al. (2011) provide evidence for an additional source of free-free emission in the form of highly collimated polar jets. Jets are typically associated with less evolved objects where luminosity is dominated by accretion processes whereas MWC 297 is considered to be a Class III / ZAMS star where the majority of the disk has fallen onto the star or been dissipated by winds.

X-ray flares are thought to be a signature of episodic accretion and Damiani et al. (2006) detect a number of X-rays flares from the Serpens MWC 297 region but find that only 5.5 per cent of total flaring is directly associated with MWC 297, suggesting that accretion onto it is minimal. The majority of X-ray emission is associated with additional YSOs and the companion of MWC 297, *OSCA*, an A2V star identified by Habart et al. (2003) and Vink et al. (2005) at a separation of 850 AU.

Figure 1.4 and Figure 1.5 show that free-free emission due to an UCHII region and polar winds/jets is responsible for the majority of flux from the star MWC 297. Original peak fluxes of 188±16 mJy and 86±22 mJy. Residual dust peak fluxes are 51 ± 10 mJy and 15 ± 3 mJy flux per pixel at 450 μm and 850 μm respectively and are highlighted in Figure 1.4 as the flux above the free-free power law fit of $\alpha = 1.03 \pm 0.02$. Free-free subtraction increases the residual dust spectral index by 35%. This corresponds to approximately 73±5 per cent and 82±4 per cent of the 450 μm and 850 μm peak flux respectively. Given our estimate of 13 per cent CO contamination, dust emission could potentially account for as little as 5 per cent of peak emission at 850 μm.

The 5σ level of 82 mJy and 11 mJy means that flux is too uncertain to be detected at 450 μm and therefore it is not possible to calculate reliable temperatures of the residual circumstellar envelope/disk around the star. The assumption of point-like free-free emission may add further uncertainty to the residual flux. We cannot say whether any dust emission contributes at the position of MWC 297.

Table 1.3: Summary of free-free contributions to SCUBA-2 wavelengths from bright objects in W40. The uncertainty on flux density at 450 μm is 0.017 Jy and 850 μm is 0.0025 Jy.

	3.6 cm (Jy)	450 μm (Jy)				850 μm (Jy)				
Object	VLA[a]	SCUBA-2	Free-free	Dust	%	SCUBA-2	Free-free	Dust	%	$\alpha_{\rm ff}$
OS1[b]	0.00578	-	-	-	-	0.101	0.064	0.038	62	0.6
OS2a	0.00240	1.83	0.16	1.67	9	0.558	0.069	0.489	12	1.0

[a] VLA 3.6 cm compact object fluxes (Rodríguez et al., 2010).
[b] OS1 covers a cluster for stellar objects where OS1a(North), VLA-12, VLA-14, VLA-16 are all radio emitters. The flux of the most prominent source, VLA-14, is included in this table but in reality the SCUBA-2 free-free flux of OS1 is a combination of all 4 of these objects.

1.6 The free-free contribution in the W40 complex results and discussion.

The W40 complex contains a number of massive stars that are detected in high resolution VLA 3.6 cm observations. A large-scale H II region is also observed at lower resolution 21 cm observations.

Figure 1.6 shows how the SCUBA-2 data is subsequently aligned and convolved to the larger resolution of the VLA 21 cm data so the two data sets are directly comparable. Given that free-free emission from the large scale H II region is essentially flat in spectrum, it is not surprising that the contribution is very limited. Peak 21 cm flux density is 0.0298 Jy/pix which corresponds to 0.0163 and 0.0174 Jy/pix at 450 and 850 μm given a spectral index of $\alpha_{\rm ff}$ = -0.1. The contribution of this peak flux to the SCUBA-2 observations is 5% at 850 μm and 0.5% at 450 μm. As a result the dust spectral index for the peak increases by 2% from 3.46 to 3.53.

3.6 cm fluxes for OS1 and OS2a are extrapolated up to SCUBA-2 wavelengths (Table 1.3) assuming an indirectly estimated free-free spectral index of 0.6 and 1.0 respectively. Modelled as a point source, the free-free emission from each star is convolved with the JCMT beam using primary and secondary components for comparison with the SCUBA-2 data (Figure 1.7). The contribution of the free-free in OS1a at 850 μm is 62% (no detection at 450 μm). The free-free contribution for OS2a is 9% at 450 μm and 12% at 850 μm. As a result the dust spectral index for the peak increases by 3%.

Having accounted for possible CO and free-free contamination, the residual flux detected from OS2a is 1.67 and 0.489 Jy at 450 μm and 850 μm respectively. We find that this gives OS2a an usually low spectral index of 1.6±0.1. Whilst lower αs have previous been explained by very low β associated with grain growth (Manoj et al., 2007), given a β=1.0, typical for circumstellar disks, an α = 1.6 would require a temperature of less than 2 K. Alternatively, an exceptionally low β approaching 0.0 would still require a temperature of less than 7 K. In both scenarios, dust temperatures this low have never been observed. Therefore the results calculated for OS2a should be considered with a high degree of scepticism.

In summary, the free-free contribution at SCUBA-2 wavelengths is limited (less that 5%) at large scales. At smaller scales it may have a small, but significant (9% to 12%) impact on prominent SCUBA-2 sources such as OS2a and a significant impact (62%) on faint SCUBA-2

sources such as OS1a. Subtraction of the free-free emission from SCUBA-2 observations acts to increase the dust spectral index, by 2% at the peak of large-scale emission and 3% from OS2b.

1.7 Conclusions

In this chapter we have examined the impact of free-free contamination on SCUBA-2 observations of star-forming regions of Serpens MWC 297 and the W40 complex. We find a small number of cases in the literature where radio-bright YSOs have free-free emission that is optically thick at submillimetre wavelengths and contributes to SCUBA and SCUBA-2 observations in addition to dust. We develop techniques that are used to subtract this small scale emission from the submillimetre observations and measure the residual dust flux and estimate the contamination fraction. Where insufficient radio observations exist to directly calculate $\alpha_{\rm ff}$ we asses the physical characteristics of individual sources to make a judgement on wether they are UCH II regions ($\alpha_{\rm ff}$ = 0.6) or collimated jets ($\alpha_{\rm ff}$ = 1.0). We also apply the same method to large scale, diffuse H II regions with an $\alpha_{\rm ff}$ = -0.1 to investigate.

Our results are summarised as:

1. The B1.5ve Herbig HAeBe star MWC 297 in the Serpens MWC 297 region has a free-free spectral index of $\alpha_{\rm ff}$ = 1.03±0.02, consistent with collimate jet geometry. SCUBA-2 peak fluxes of 188±16 mJy and 86±22 mJy are consistent with an outstanding point source at the location of MWC 297 inferring that free-free emission from the ZAMS-star maybe optically thick at submillimetre wavelengths.

2. Free-free emission from MWC 297 was found to contribute to approximately 73±5 per cent and 82±4 per cent of the 450 μm and 850 μm peak flux respectively. Residual dust peak fluxes are 51±10 mJy and 15±3 mJy flux per pixel at 450 μm and 850 μm respectively. Subtracting the free-free emission increases the spectral dust index by 35%. Dust at 850 μm represents a 1.4σ detection and at 450 μm a 0.6σ detection confirming that any residual disc around MWC 297 is too faint to be reliably detected.

3. A number of radio bright stars are observed in the W40 complex in the IR. OS1b, c, OS3a and IRS 5 are not detected in SCUBA-2, confirming that any free-free emission from these objects is optically thin at submillimetre wavelengths and no contamination subtraction is required.

4. The O9.5 MS-star OS1a and a cluster members VLA 12, 14 and 15 are non-variable compact radio sources with no evidence jet features observed. We classify these as UCH II regions with $\alpha_{\rm ff}$ = 0.6 and calculate a free-free contribution of 62% at 850 μm (no detection at 450 μm).

5. The Herbig AeBe star OS2a has a variable compact radio source consistent with episodic accretion. Radio shock fronts are also observed in the vicinity that would be consistent with jet emission. A significant SCUBA-2 peak of 1.83 and 0.558 Jy at 450 μm and 850 μm respectively is associated with this object. We classify this object as a collimated jet with

an $\alpha_{\rm ff}$ = 1.0 and calculate a free-free contribution of 9% at 450 μm and 12% at 850 μm. Subtracting the free-free emission increases the spectral dust index by 2%. The residual dust has an unusually low spectral index 1.6±0.1 which is is difficult to explain without invoking exceptional cold dust temperatures.

6. The B4 star OS2b has a variable compact radio source consistent with episodic accretion but lacks any signatures of jet emission. If a weak UCH II region is being detected it would be consistent with the B4 spectral class of the star which lies right on the threshold of sufficient Lyman photon production to power an H II region. We therefore judge that any free-free emission from this star would optically thin at SCUBA-2 wavelengths.

7. The large, diffuse H II region is observed in the W40 complex. This feature has an $\alpha_{\rm ff}$ = -0.1 and has a peak flux of 0.03 Jy/pix in 21 cm VLA data which has a free-free contribution of 0.5% at 450 μm and 5% at 850 μm. Subtracting the free-free emission increases the spectral dust index by 3%.

   Our results lead us to believe that where free-free emission is sufficiently bright and optically thick its contribution can lead to the observation of prominent point sources and significantly lower dust spectral indices, and therefore temperatures. Where the free-free emission is less prominent, in faint UCH II regions and from large-scale H II it can still have a limited, if non-negligible impact on the dust spectral index. In the following chapter we will look at what quantifiable affects the free-free emission has when examining the dust temperature.

Bibliography

Alonso-Albi T., Fuente A., Bachiller R., Neri R., Planesas P., Testi L., Berné O., Joblin C., 2009, A&A, 497, 117

Altenhoff W. J., Downes D., Goad L., Maxwell A., Rinehart R., 1970, A&AS, 1, 319

Condon J. J., Kaplan D. L., 1998, VizieR Online Data Catalog, 211, 70361

Dale J. E., Bonnell I., 2011, MNRAS, 414, 321

Dale J. E., Bonnell I. A., Clarke C. J., Bate M. R., 2005, MNRAS, 358, 291

Dale J. E., Ercolano B., Bonnell I. A., 2012, MNRAS, 424, 377

Damiani F., Micela G., Sciortino S., 2006, A&A, 447, 1041

Drew J. E., Busfield G., Hoare M. G., Murdoch K. A., Nixon C. A., Oudmaijer R. D., 1997, MNRAS, 286, 538

Greenstein J. L., 1973, ApJL, 184, L23

Habart E., Testi L., Natta A., Vanzi L., 2003, A&A, 400, 575

Harvey P. M., Thronson Jr. H. A., Gatley I., 1979, ApJ, 231, 115

Kurtz S., 2005, in Cesaroni R., Felli M., Churchwell E., Walmsley M., eds, Massive Star Birth: A Crossroads of Astrophysics Vol. 227 of IAU Symposium, Hypercompact HII regions. pp 111–119

Kurtz S., Churchwell E., Wood D. O. S., 1994, ApJS, 91, 659

Lefloch B., Lazareff B., 1994, A&A, 289, 559

Malbet F., Benisty M., de Wit W.-J., Kraus S., Meilland A., Millour F., Tatulli E., Berger J.-P., Chesneau O., Hofmann K.-H., Isella A., Natta A., Petrov R. G., Preibisch T., Stee P., Testi L., Weigelt G., Antonelli P., Beckmann U., 2007, A&A, 464, 43

Manoj P., Ho P. T. P., Ohashi N., Zhang Q., Hasegawa T., Chen H.-R., Bhatt H. C., Ashok N. M., 2007, ApJL, 667, L187

McKee C. F., Tan J. C., 2003, ApJ, 585, 850

Mezger P. G., Henderson A. P., 1967, ApJ, 147, 471

Molinari S., Brand J., Cesaroni R., Palla F., Palumbo G. G. C., 1998, A&A, 336, 339

Olnon F. M., 1975, A&A, 39, 217

Oster L., 1961, ApJ, 134, 1010

Panagia N., Felli M., 1975, A&A, 39, 1

Reynolds S. P., 1986, ApJ, 304, 713

Rodney S. A., Reipurth B., 2008, The W40 Cloud Complex. p. 683

Rodríguez L. F., Rodney S. A., Reipurth B., 2010, AJ, 140, 968

Rodríguez L. F., Zapata L. A., Dzib S. A., Ortiz-León G. N., Loinard L., Macías E., Anglada G., 2014, ApJL, 793, L21

Rumble D., Hatchell J., Gutermuth R. A., Kirk H., Buckle J., Beaulieu S. F., Berry D. S., Broekhoven-Fiene H., 2015, MNRAS, 448, 1551

Sandell G., Weintraub D. A., Hamidouche M., 2011, ApJ, 727, 26

Shuping R. Y., Vacca W. D., Kassis M., Yu K. C., 2012, AJ, 144, 116

Skinner S. L., Brown A., Stewart R. T., 1993, ApJS, 87, 217

Smith J., Bentley A., Castelaz M., Gehrz R. D., Grasdalen G. L., Hackwell J. A., 1985, ApJ, 291, 571

Tafoya D., Gómez Y., Rodríguez L. F., 2004, ApJ, 610, 827

Thompson M. A., White G. J., Morgan L. K., Miao J., Fridlund C. V. M., Huldtgren-White M., 2004, A&A, 414, 1017

Urquhart J. S., Morgan L. K., Thompson M. A., 2009, A&A, 497, 789

Vink J. S., O'Neill P. M., Els S. G., Drew J. E., 2005, A&A, 438, L21

Walsh A. J., Burton M. G., Hyland A. R., Robinson G., 1998, MNRAS, 301, 640

Wood D. O. S., Churchwell E., 1989, ApJS, 69, 831

Wright A. E., Barlow M. J., 1975, MNRAS, 170, 41

Yorke H. W., Tenorio-Tagle G., Bodenheimer P., Rozyczka M., 1989, A&A, 216, 207